PAPER

Check for updates

Single-step wet-chemical fabrication of sheet-type electrodes from solid-electrolyte precursors for all-solid-state lithium-ion batteries†

Dae Yang Oh, Dong Hyeon Kim, Sung Hoo Jung, Jung-Gu Han, Nam-Soon Choi [ID] and Yoon Seok Jung [ID] *

All-solid-state lithium-ion batteries (ASLBs) employing sulfide solid electrolytes (SEs) have emerged as promising next-generation batteries for large-scale energy storage applications in terms of safety and high energy density. While slurry-based fabrication processes using polymeric binders and solvents are inevitable to produce sheet-type electrodes, these processes for ASLBs have been overlooked until now. In this work, we report the first scalable single-step fabrication of bendable sheet-type composite electrodes for ASLBs using a one-pot slurry prepared from SE precursors (Li_2S and P_2S_5), active materials ($LiNi_{0.6}Co_{0.2}Mn_{0.2}O_2$ or graphite), and polymeric binders (nitrile-butadiene rubber (NBR) or polyvinyl chloride (PVC)) *via* a wet-chemical route using tetrahydrofuran. At 30 °C, the $LiNi_{0.6}Co_{0.2}Mn_{0.2}O_2$ and graphite electrodes wet-tailored from SE precursors and NBR exhibit high capacities of 140 mA h g^{-1} at 0.1C and 320 mA h g^{-1} at 0.2C, respectively. Particularly, the rate capability of the graphite electrode in an all-solid-state cell is superior to that of a liquid electrolyte-based cell. Additionally, the effects of the size of the SE precursors and the polymeric binders on the electrochemical performance are investigated. Finally, the excellent electrochemical performance of $LiNi_{0.6}Co_{0.2}Mn_{0.2}O_2$/graphite ASLBs assembled using the as-single-step-fabricated electrodes are also demonstrated not only at 30 °C but also at 100 °C.

Introduction

The high energy density provided by lithium-ion batteries (LIBs) allowed them to increasingly conquer the market for portable electronic devices over the past 20 years.[1,2] Recently, LIBs are expanding their footprint to large-scale energy storage applications such as electric vehicles (EVs) and smart grids.[2] However, the use of organic liquid electrolytes poses serious safety concerns, such as flammability and leakage, thereby threatening ongoing and future applications of LIBs.[1] Replacement of the organic liquid electrolytes with non-flammable inorganic solid electrolytes (SEs) could provide an ideal solution.[3–9] Additionally, retaining the composite structure of LIB electrodes while employing solidified electrolytes offers significant advantages in terms of scalable fabrication (*e.g.*, the use of active materials and SEs in their powder forms, as well as slurry-based methods) and high energy density.[5,10,11] Thus, so-called "bulk-type" all-solid-state lithium-ion batteries (ASLBs) based on composite structures have attracted much attention.[3–5,10,11]

School of Energy and Chemical Engineering, Department of Energy Engineering, Ulsan National Institute of Science and Technology (UNIST), Ulsan 44919, South Korea. E-mail: ysjung@unist.ac.kr

† Electronic supplementary information (ESI) available. See DOI: 10.1039/c7ta06873e

SEs are key to the success of bulk-type ASLBs, and despite their instability in air,[10] sulfide-based SE materials are one of the most promising candidates because of two exceptional advantageous features. First, the deformability of sulfide materials allows two-dimensional contacts to be made with the active materials by a simple mechanical pressing process at room temperature, in contrast with brittle oxide-based materials.[5,12] Second, several state-of-the-art sulfide SEs exhibit much higher ionic conductivity (*e.g.*, $Li_{10}GeP_2S_{12}$-structured derivatives:[3,4] max. 2.5×10^{-2} S cm^{-1}, $Li_7P_3S_{11}$:[13,14] 1.7×10^{-2} S cm^{-1}, Li_6PS_5X (X = Cl, Br, I):[15] $\geq 1 \times 10^{-3}$ S cm^{-1}) than their oxide counterparts (*e.g.*, $Li_7La_3Zr_2O_{12}$:[16] 10^{-4}–10^{-3} S cm^{-1}), which can be rationalized by the increased ionic size and polarizability of the sulfide ion compared to the oxide ion.[17] A drawback of sulfide materials is their lower stability to electrochemical oxidation than the oxide materials.[18,19] The lability of sulfide SEs at high voltages and their chemical reactivity with cathode materials leads to poor electrochemical performance when combined with conventional cathode materials such as $LiMO_2$ (M = Co, Ni, Mn).[5,20] However, introducing a protective layer such as $LiNbO_3$ and $Li_4Ti_5O_{12}$ between the $LiMO_2$ and the sulfide SE significantly improves the interfacial stability.[3–5,20,21]

Previously reported efforts to synthesize sulfide SE materials have focused on the exploration of new compositions and structures, overlooking new synthesis protocols.[3–5,13,15] Recently,

This journal is © The Royal Society of Chemistry 2017

J. Mater. Chem. A, 2017, 5, 20771–20779 | 20771

β-Li$_3$PS$_4$ was reported to be prepared using tetrahydrofuran (THF),[22] and showed a conductivity of 1.6×10^{-4} S cm^{-1}. This result initiated the subsequent research on wet-chemical syntheses of sulfide SEs using liquid solvents, *e.g.*, Li$_7$P$_2$S$_8$I using acetonitrile (6.3×10^{-4} S cm^{-1}),[23] 0.4LiI–0.6Li$_4$SnS$_4$ using methanol (4.1×10^{-4} S cm^{-1}),[10] Li$_7$P$_3$S$_{11}$ using acetonitrile (9.7×10^{-4} S cm^{-1}),[24] and Na$_3$SbS$_4$ using methanol or water ($\sim 2 \times 10^{-4}$ S cm^{-1}).[11] These wet-chemical syntheses provided several new opportunities. First, these routes may provide new SE materials with high conductivity that otherwise could not be produced by conventional synthesis protocols. For example, β-Li$_3$PS$_4$ prepared using THF (1.6×10^{-4} S cm^{-1})[22] and a 0.4LiI–0.6Li$_4$SnS$_4$ glass (4.1×10^{-4} S cm^{-1}) obtained from a methanol solution[10] cannot be prepared by conventional high-temperature solid-state syntheses. Second, the wetting of the active materials by SEs could be enhanced using a wet-chemical SE synthesis.[10,11,25,26] Recently, our group demonstrated that directly coating the highly conductive SEs 0.4LiI–0.6Li$_4$SnS$_4$ and Na$_3$SbS$_4$ onto active materials, such as LiCoO$_2$ and NaCrO$_2$, by the solution-process could significantly enhance the electro-chemical performance of all-solid-state Li- or Na-ion batteries, respectively. Third, the cost-effective mass production of SEs could be facilitated by a wet-chemical synthesis using SE precursors, such as Li$_2$S, P$_2$S$_5$, and LiX (X = Cl, Br, I), and cheap solvents. Lastly, the size and morphology of the SE particles may be controllable by optimizing the wet-chemical synthetic

conditions, which would directly relate to the quality of ionic contacts and connections in the composite electrodes of ASLBs.[27–30]

The fabrication protocols for the assembly of bulk-type ASLBs in most previous reports are based on dry-mixing of the active materials, SEs, and conductive additives powders.[3,5,6,10–12,18,21] However, the resulting pelletized cells are difficult to scale up for practical applications, such as for large-format batteries employing sheet-type electrodes, because of their mechanically unstable features.[31] The introduction of a small amount of a polymeric component would be necessary to scale up their production, and reports of relevant examples of such approaches are very scarce. Recently, our group reported free-standing ASLBs based on bendable $\sim$70 μm-thick SE films produced using a polymeric nonwoven sheet as a mechanically compliant scaffold.[31] The fabrication of composite electrodes for ASLBs using polymeric binders such as nitrile-butadiene rubber (NBR), styrene-butadiene rubber (SBR), and silicone rubber has also been reported previously.[32,33]

We report the first instance of a scalable single-step fabrication of bendable sheet-type composite electrodes for ASLBs using a one-pot slurry prepared from SE precursors (Li$_2$S and P$_2$S$_5$), active materials (LiNi$_{0.6}$Co$_{0.2}$Mn$_{0.2}$O$_2$ (NCM622) or graphite), and polymeric binders (NBR or polyvinyl chloride (PVC)) *via* a wet-chemical route using THF. The single-step process using SE precursors, rather than SEs, and polymeric
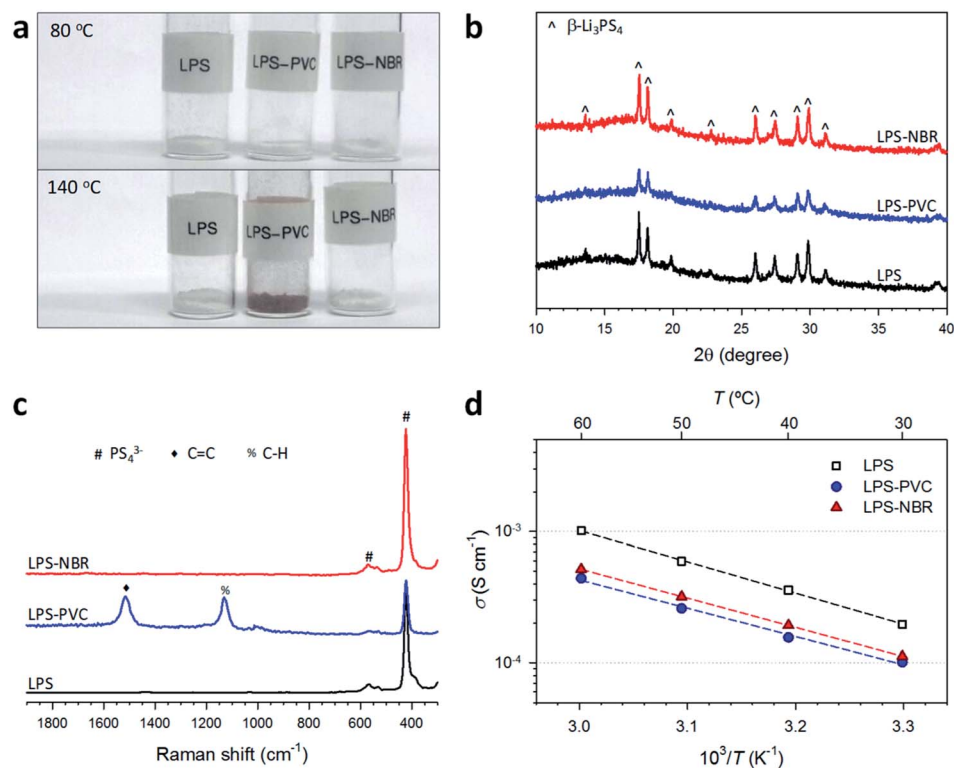
Fig. 1 Characterization of SE (LPS)–polymeric binder composites prepared *via* a wet-chemical synthesis using THF. (a) Photographs of the SE-polymeric binder composites after heat treatment at 80 °C and 140 °C. (b) XRD patterns, (c) Raman spectra, and (d) Arrhenius plots of the Li-ion conductivities of pristine SE (LPS) and SE-polymeric binder composites (LPS-PVC and LPS-NBR). The *y*-axis is shown in log scale. The SE-polymeric binder composites were prepared by heat treatment at 140 °C. The weight ratio of LPS/polymer was 94.5 : 5.5.

binders offers a significant advantage for practical applications. At 30 °C, the single-step-fabricated electrodes exhibit a capacity of 140 mA h g^{-1} at 0.1C for NCM622 and 320 mA h g^{-1} at 0.2C for graphite. The excellent electrochemical performance of NCM622/graphite ASLBs assembled using the single-step-fabricated electrodes are also demonstrated at an extremely high temperature of 100 °C as well as at 30 °C. Additionally, the reliance of the electrochemical performance on the particle size of the SE precursors and polymeric binders are investigated.

Results and discussion

Compatibility between SE (Li$_3$PS$_4$) and polymeric binders (PVC and NBR)

Three samples were prepared to assess the compatibility of SEs and polymeric binders during the wet-chemical process. Pristine Li$_3$PS$_4$ (LPS) was prepared by reacting powders of its two precursors Li$_2$S and P$_2$S$_5$ in THF, followed by a treatment under vacuum at 80 °C and a subsequent heat treatment under vacuum at 140 °C. The severe reactivity of sulfide materials with polar solvents meant that less polar solvents such as toluene and xylene were typically used to fabricate electrodes using sulfide SEs by conventional wet methods.[31,34,35] These solvents severely restricted the available polymeric binders to the few that are soluble in less polar solvents (*e.g.*, NBR, SBR).[32,33] In contrast, our use of THF to prepare LPS ensures the compatibility of this protocol with a wide range of polymeric binders. The THF-soluble binders NBR and PVC were selected as model polymers. LPS-polymeric binder composites were prepared using the same wet-chemical route as for pristine LPS except that the polymers (5.5 wt%) were dissolved in THF solutions containing Li$_2$S and P$_2$S$_5$. The LPS-polymer binder composite samples are referred to as LPS-NBR and LPS-PVC.

Fig. 1a shows photographs of the LPS and LPS-polymer composite powders after heat treatments at 80 °C and 140 °C. No significant changes in appearance were observed between the cases for heat treatment at 80 °C and 140 °C for LPS and LPS-NBR. In contrast, the LPS-PVC powders, which were white after a heat-treatment at 80 °C, changed to violet after heat treatment at 140 °C, indicating the occurrence of chemical changes. The thermal decomposition of PVC, resulting in the formation of a C=C double bond with release of HCl, is well known (Fig. S1, ESI†).[36] While pristine PVC is thermally stable up to 240 °C, PVC processed by dissolving into THF started to decompose at ~80 °C (Fig. 2a). The traces of free radicals formed from THF likely initiated dehydrochlorination of PVC.[36] Thus, the significant change in color of LPS-PVC after heat treatment at 140 °C is caused by the thermal decomposition (or dehydrochlorination) of PVC. In contrast, both the pristine and THF-treated NBR showed good thermal stability up to 320 °C under Ar (Fig. 2a). LPS, LPS-PVC, and LPS-NBR were further compared using X-ray diffraction (XRD) and Raman spectroscopy. The XRD patterns of LPS, LPS-PVC, and LPS-NBR, shown in Fig. 1b, closely match β-Li$_3$PS$_4$ without any impurity phases.[22,37] However, in the case of LPS-PVC, the overall peak intensities are lower than for LPS or LPS-NBR. We suggest that the HCl generated by thermal decomposition of PVC during heat treatment may react with
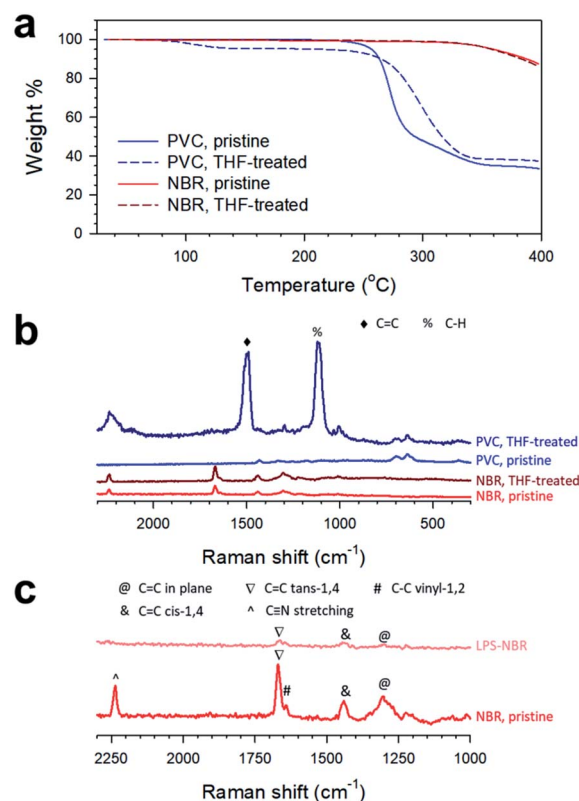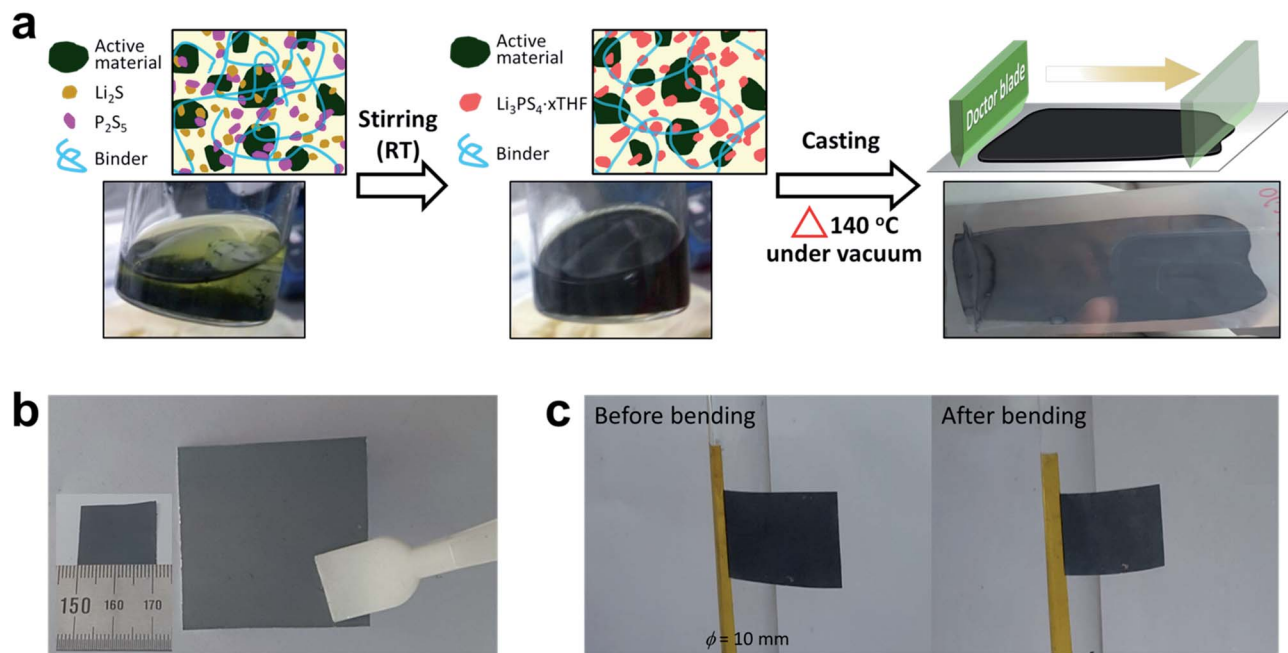
Fig. 2 Characterization of pristine and THF-treated polymers (PVC and NBR). (a) TGA profiles of the pristine and THF-treated PVC and NBR under Ar. The THF-treated polymers were prepared by dissolving the pristine polymers in THF and subsequently evaporating the THF under vacuum at 80 °C. Raman spectra of (b) the pristine and THF-treated PVC and NBR, and (c) pristine NBR and LPS-NBR.

sulfides, hindering the formation of Li$_3$PS$_4$. The Raman spectra of LPS, LPS-PVC, and LPS-NBR are shown in Fig. 1c, and exhibit the characteristic signals of PS$_4$$^{3-}$ (labeled "#"). However, the spectrum for LPS-PVC is distinctly different from those of LPS and LPS-NBR; the strong peaks at 1515 cm^{-1} (labeled "◆") and 1131 cm^{-1} (labeled "%") originate from C=C stretching and C–H in-plane vibration, respectively, indicating the dehydrochlorination of PVC in LPS-PVC (Fig. S1, ESI†).[38] These peaks were also found in the THF-treated PVC, implying that the dehydrochlorination of PVC is associated with a history of interaction with THF (Fig. 2b and c).[36] In sharp contrast, the characteristic peaks for NBR were retained for both LPS-NBR and THF-treated NBR, confirming the excellent compatibility of NBR with sulfide SEs during the wet-chemical fabrication and the subsequent heat treatments (Fig. 2b and c).

Fig. 1d shows an Arrhenius plot of the Li$^+$ ionic conductivity of LPS, LPS-PVC, and LPS-NBR, measured using Li-ion blocking Ti/SE/Ti symmetric cells (typical Nyquist plots are shown in Fig. S2, ESI†). Pristine LPS had a conductivity of 2.0 × 10^{-4} S cm^{-1} at 30 °C, which agrees with a previously reported value.[22] After the formation of a composite with 5.5 wt% of the polymeric binders (LPS-PVC and LPS-NBR), the conductivity was decreased by ~50% (~1 × 10^{-4} S cm^{-1}), which was attributed to the Li-ion insulating nature of polymers. However,
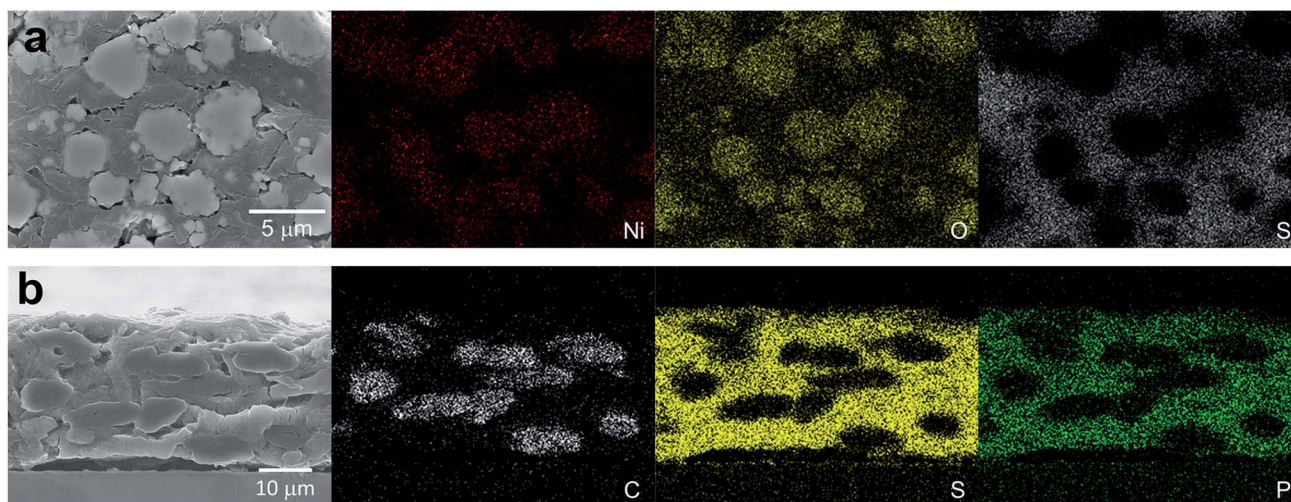
Fig. 3 Sheet-type composite electrodes prepared from SE precursors *via* a single-step wet-chemical route. (a) Schematic diagram illustrating the single-step wet-fabrication of sheet-type composite electrodes. Photographs of the one-pot slurry and the as-fabricated electrode in each step are shown. Conductive additives (super C65) are not shown in the scheme. (b) Photographs of the as-prepared electrode. (c) Photographs of the electrode before and after bending tests. The NCM622 electrodes are shown in the photographs.

a conductivity of 1×10^{-4} S cm^{-1} is high enough to operate ASLBs at room temperature.[10]

Single-step wet-chemical fabrication of electrodes

A single-step process for the fabrication of composite electrodes *via* a wet-chemical route is illustrated in Fig. 3a. A slurry was prepared in one-pot by adding the active materials (NCM622 or graphite), SE precursors (Li$_2$S and P$_2$S$_5$), polymeric binders (NBR or PVC), and carbon additives (Super C65) to THF. The resulting homogeneous and viscous slurry was cast and

uniformly coated on the current collectors (Al and Ni foils for NCM622 and graphite electrodes, respectively) by the doctor blade method, which is representative of the fabrication protocol for conventional LIB-electrodes. The subsequent heat treatment under vacuum allows the solvent (THF) to evaporate and forms a highly conductive SE, Li$_3$PS$_4$ (from Li$_3$PS$_4$·xTHF).[22] Photographs of the as-prepared electrodes are shown in Fig. 3a and b, which show that the electrode layers were uniformly coated. Importantly, the electrodes exhibited no damage after repeated bending, indicating the good adhesion of the electrode

Fig. 4 Electron microscopy characterization of cross-sectioned wet-chemically fabricated electrodes. Cross-sectional FESEM images of the single-step wet-chemically fabricated (a) NCM622 and (b) graphite electrodes and their corresponding EDXS elemental maps.
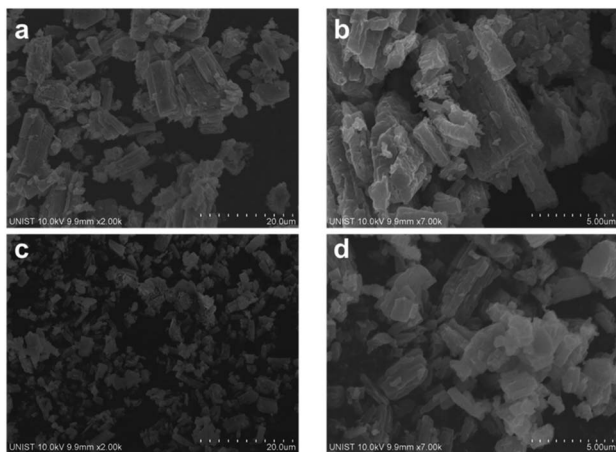
Fig. 5 FESEM images of LPS powders prepared from (a, b) the pristine precursors (PP) and (c, d) the ball-milled precursors (BP).

layers to the Al foil (Fig. 3c and S3, ESI†). The single-step-fabricated electrodes could thus be applied to scalable roll-to-roll process for practical application.[31] The bendability and adhesion emphasize the positive role of polymeric binders. Fig. 4 shows cross-sectional field-emission scanning electron microscopy (FESEM) images of the single-step wet-chemically fabricated NCM622 and graphite electrodes, and their corresponding energy dispersive X-ray spectroscopy (EDXS) elemental maps (more FESEM images and elemental maps for the NCM622 electrode are also provided in Fig. S4, ESI†).

The size distribution of the SEs can affect the electrochemical performances of ASLBs in terms of the quality of their ionic contacts and percolation.[27–30] We found that the particle size of the SE precursors (Li_2S and P_2S_5) led to that of the resulting SE *via* the wet-chemical synthesis. The LPS powders that were formed from ball-milled precursors showed smaller particle sizes (~1 μm) than those formed from the pristine precursors (~10 μm, Fig. 5). Thus, three electrodes were prepared and compared; BP-PVC, BP-NBR, PP-NBR. For example, BP-NBR indicates the electrode prepared by using the ball-milled SE precursors and NBR.

Electrochemical performances of single-step wet-chemically fabricated electrodes

The electrochemical performances at 30 °C of electrodes fashioned by the single-step wet-chemical protocol were assessed in NCM622/Li–In and graphite/Li–In all-solid-state half-cells, and their results are shown in Fig. 6. The NCM622 electrode with BP-NBR in the all-solid-state cell (Fig. 6a) showed a capacity of 153 mA h g^{-1} at 0.05C. This value is lower than that of a liquid electrolyte cell (160 mA h g^{-1} at 0.2C, Fig. S5a, ESI†), which were attributed to the low ionic conductivity of LPS, interfacial resistance, and imperfections in the ionic contacts and percolations.[10,11,20,26,34] However, a capacity of 153 mA h g^{-1} is a high value compared to the cathode materials in previously reported ASLBs.[5,10,33,34,39] The rate capability of NCM622 electrodes are compared in Fig. 6b and c. The performance of BP-NBR was superior to that of BP-PVC, which is attributed to the differences in the inertness of NBR and PVC during the wet-chemical fabrication of electrodes. Furthermore, BP-NBR outperformed PP-NBR, indicating that an SE with a smaller particle size is desirable to improve the ionic contact and percolation.[27–30] The
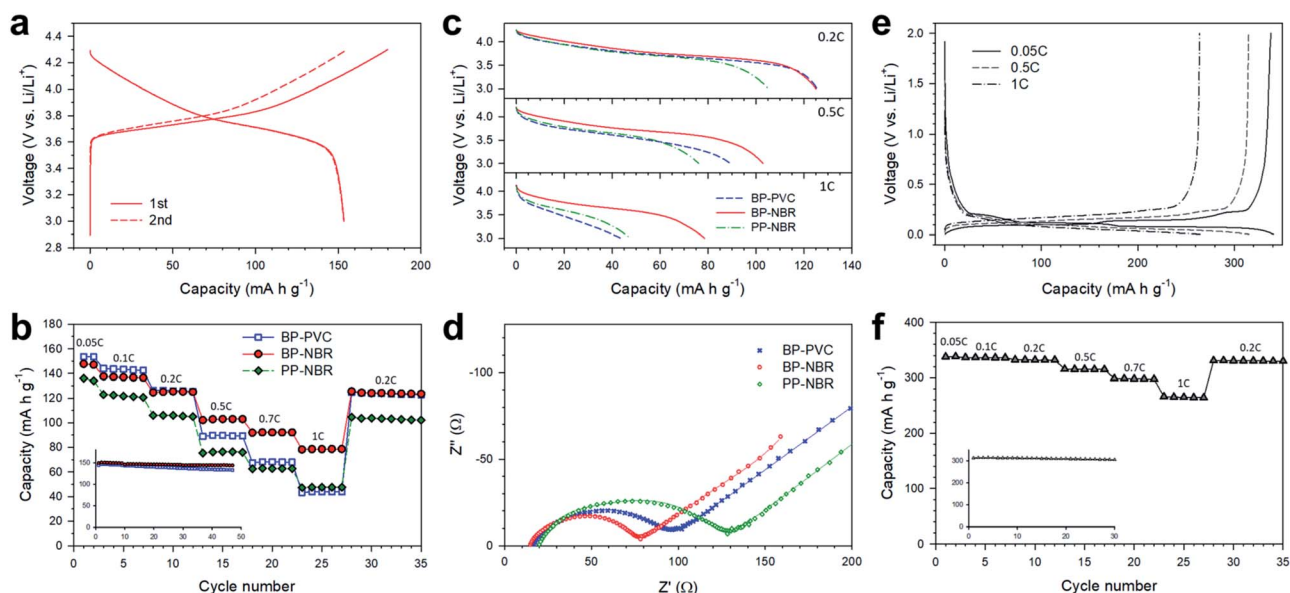

Fig. 6 Electrochemical characterization for NCM622/Li–In and graphite/Li–In all-solid-state cells at 30 °C, employing sheet-type composite electrodes prepared from one-pot slurry *via* the wet-chemical process. (a) First- and second-cycle voltage profiles for the NCM622 electrode prepared from ball-milled LPS precursors and NBR (BP-NBR) at 0.05C. (b) Rate capabilities of the NCM622 electrode, varied by ball-milling of SE precursors and polymeric binders. (c) Discharge voltage profiles and (d) Nyquist plots for the NCM622 electrodes. The solid lines in (d) are the fitted results based on the equivalent circuit model shown in Fig. S7 (ESI†). (e) Charge–discharge voltage profiles and (f) rate capability of the graphite electrode prepared from ball-milled LPS precursors and NBR (BP-NBR). The cycle performances of NCM622 and graphite electrodes are shown in the insets of (b) and (f), respectively.

This journal is © The Royal Society of Chemistry 2017

J. Mater. Chem. A, 2017, **5**, 20771–20779 | **20775**

surface coverage of SEs on NCM622 particles was investigated by analysis of galvanostatic intermittent titration technique (GITT) data (Fig. S6, see the ESI† for details). The BP-NBR electrode exhibited a higher surface coverage of SE (14%) than PP-NBR (10%), which agrees well with the superior rate capability of BP-NBR to that of PP-NBR. The very low surface coverage values are attributed to incomplete wetting of NCM622 by the SEs,[10,11] and the presence of inaccessible inner pores in the NCM622 particles.[40] The Nyquist plots in Fig. 6d also agree with the trend in the rate performance; the amplitudes of the semicircles decrease in the order of PP-NBR (105.7 Ω), BP-PVC (74.1 Ω), and BP-NBR (58.8 Ω).

The excellent rate capability of graphite electrodes with BP-NBR is shown by the voltage profiles and charge capacities at different C-rates in Fig. 6e and f. The capacity retention of graphite-BP-NBR capacity at 1C was 79% (265 mA h g^{-1}) of the capacity at 0.05C (338 mA h g^{-1}). It is surprising that the rate performance of graphite in an all-solid-state cell significantly outperformed that in a liquid electrolyte cell (only 42% of the capacity (148 mA h g^{-1}) is retained at 1C, compared to the capacity at 0.05C; Fig. S5b, ESI†). This result is in stark contrast with that of NCM622 (Fig. 6b and S5a, ESI†), for which the LE-cell outperformed the SE-cell. The superior rate capability of graphite to NCM622 in all-solid-state cells may be rationalized by considering several factors: (i) the good compatibility between graphite and LPS, in contrast to the interatomic diffusion or chemical reaction that occur between LiCoO$_2$ and sulfide SEs.[19,20] (ii) The absence of conductive additives in the graphite electrode in the all-solid-state cell, which allows the formation of favorable ionic conduction pathways.[18,35] Overall rate performance of ASLBs could be offset by disruption in ionic conduction pathways by carbon additives. Because graphites could form good electronic conduction pathways by themselves, no carbon additives are needed, which could maximize the ionic conduction. (iii) Possible undesirable side reactions of NCM622, caused by exposure to the Li$_2$S- and P$_2$S$_5$-containing THF solution. A control experiment confirmed that NCM622 which was exposed to a THF solution containing Li$_2$S and P$_2$S$_5$ showed a slightly inferior performance to that of pristine NCM622 (Fig. S8, ESI†). A protective ultrathin Al$_2$O$_3$ coating on NCM622 by 10 cycles of atomic layer deposition (ALD) appeared to mitigate the degradation of electrochemical performance caused by the side reaction on the surface of NCM622 during the wet-chemical process.[41–43] This result indicates that further improvements of electrochemical performance of the single-step wet-chemically fabricated NCM622 electrode would be possible.

The factors contributing to the abnormally superior rate capability of the graphite-based all-solid-state cell over the conventional liquid electrolyte-based cell, despite the SE (LPS, ~10^{-4} S cm^{-1}) having a lower conductivity than a liquid electrolyte (~10^{-2} S cm^{-1}), were further considered. The presence of SE particles in the one-pot slurry might suppress the alignment of graphite flakes on the current collectors, which is typical of the conventional LIB electrodes and results in poor rate capability.[44] The resulting reduction in the tortuosity of the graphite electrode in the all-solid-state cell could provide more favorable ionic conduction pathways.[44,45] Further, the effects

from different nature between the graphite/SE and graphite/liquid electrolyte interfaces in terms of solid electrolyte interphase (SEI) and Li$^+$ desolvation process cannot be dismissed.[4,46] As shown in the insets in Fig. 6b and f, both NCM622 and graphite electrodes cycled at 0.1C showed excellent cycling stabilities (97% of the capacity retention after 45 and 30 cycles for NCM622 and graphite, respectively).

Finally, a rocking-chair ASLB was assembled using the NCM622 and graphite electrodes fabricated by the single-step wet-chemical route. It is clearly shown that both the NCM622 and graphite electrodes form close contacts with the SE layers without any noticeable mechanical failures (Fig. S9, ESI†), highlighting good sinterability of sulfide SEs by cold-pressing. Their electrochemical performance at 30 °C and 100 °C are presented in Fig. 7. The NCM622/graphite full-cell showed a reversible capacity of 131 mA h g$_{NCM622}$$^{-1}$ in the voltage range of 2.50–4.15 V at 0.1C and 30 °C, which translates to an energy
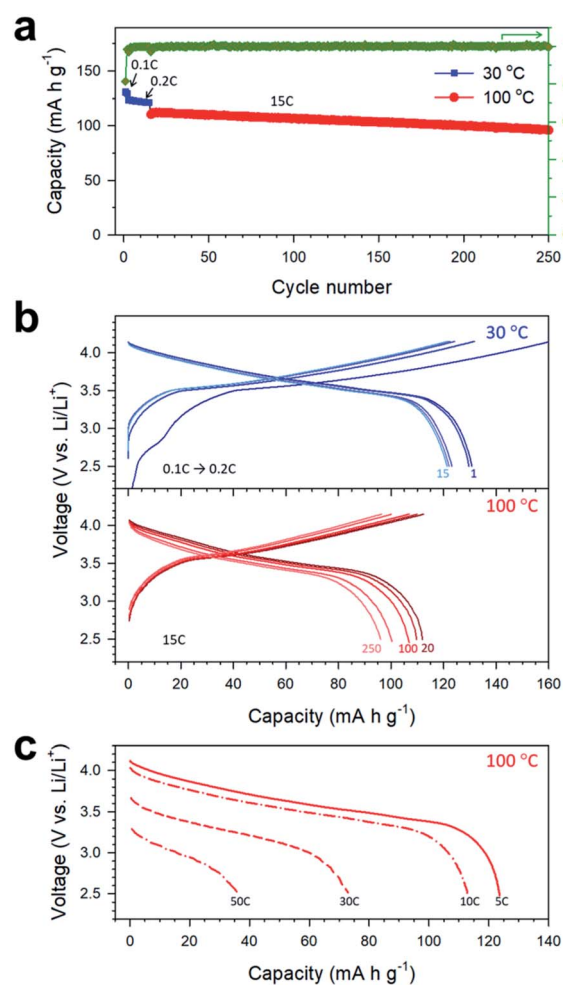

Fig. 7 Electrochemical performance of a rocking-chair ASLB at 30 °C and 100 °C, employing the NCM622 and graphite electrodes prepared *via* the single-step wet-chemical route (BP-NBR). (a) Cycle performance with coulombic efficiency and (b) the corresponding charge–discharge voltage profiles, and (c) discharge voltage profiles at different C-rates for NCM622/graphite ASLBs. The numbers in (b) indicate the cycle numbers.
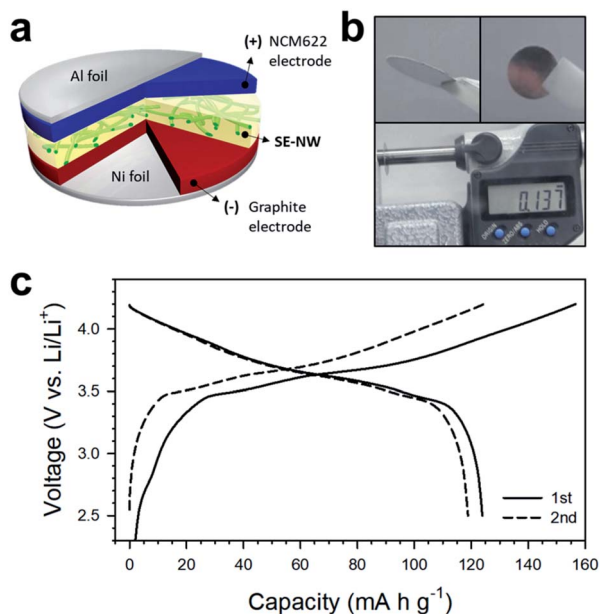
20776 | *J. Mater. Chem. A*, 2017, **5**, 20771–20779

This journal is © The Royal Society of Chemistry 2017

Fig. 8 NCM622/graphite ASLB using a thin (~70 μm) SE-NW composite film. (a) Schematic diagram and (b) the photographs of the free-standing NCM622/SE-NW/graphite ASLB. (c) The first- and second-cycle charge–discharge voltage profiles of the NCM622/SE-NW/graphite ASLB at 0.025C and 30 °C.

density of 241 W h $kg_{NCM622+graphite}^{-1}$. At 100 °C, the NCM622/graphite battery showed a high capacity of 110 mA h g_{NCM622}^{-1} at a high C-rate of 15C. 86% of the capacity was retained after 250 cycles, relative to the initial capacity at 100 °C. The coulombic efficiency was 81% at the first cycle and over 99.5% at the subsequent cycles even at 100 °C. The temperature of 100 °C is far beyond the operating temperature limits for conventional LIBs (<60 °C).[4,47] However, the NCM622/graphite ASLB showed an extremely high rate capability at 100 °C (Fig. 7c). At 30C, the full-cell showed a capacity of 73 mA h g_{NCM622}^{-1} in the voltage range of 2.5–4.2 V. While the afore-mentioned results were based on the NCM622/graphite full-cell using the conventional thick SE layer (~700 μm) in between the NCM622 and graphite electrodes, fabrication using a thin and bendable SE-nonwoven (NW) composite film (~70 μm) was also attempted.[31] The NCM/SE-NW/graphite full-cell exhibited the first-cycle reversible capacity of 124 mA h g_{NCM622}^{-1} in the voltage range of 2.5–4.2 V at 0.025C and 30 °C (Fig. 8). This preliminary result may shed light on roll-to-roll processability of fabrication protocol for ASLBs.[34] Considering the overall weight (or volume) of electrodes and SE layers, energy density of the NCM/SE-NW/graphite full-cell is calculated to be 92 W h kg^{-1} (109 W h L^{-1}).

Conclusions

In summary, a scalable single-step wet-chemical fabrication protocol for bendable sheet-type composite ASLB electrodes was successfully demonstrated. In all-solid-state cells at 30 °C, the NCM622- and graphite-based electrodes, prepared from a one-pot slurry including SE precursors and polymeric binders, exhibited capacities that were comparable to those of liquid

electrolyte cells. The rate capability of the graphite electrode in the all-solid-state cell was superior to that in the liquid electrolyte cell. We revealed that the superior electrochemical performance of NBR-based electrodes relative to PVC-based electrodes originated from the instability of PVC during the wet-chemical fabrication. Additionally, the particle size of the SE precursors affected the size of the SE particles, which in turn influenced the electrochemical performance. Finally, excellent cycling stability and rate capability were demonstrated for NCM622/graphite ASLBs at 100 °C, highlighting the exceptional advantage of ASLBs. Thus, we believe that our results provide a new protocol for producing ASLB electrodes and can contribute to progress in practical all-solid-state technologies.

Experimental

Preparation of materials

LPS and LPS-polymer composite powders were prepared by a wet-chemical method. PVC and NBR (acrylonitrile 37–39 wt%) were purchased from Sigma-Aldrich. Ball-milled Li_2S (99.9%, Alfa-Aesar) and P_2S_5 (99%, Sigma-Aldrich) (2 g each) were obtained by mechanical milling at 500 rpm for 10 h, using a planetary ball mill (Pulverisette 7PL, Fritsch) with a zirconia vial (80 mL) and twenty zirconia balls (5 mm in diameter). LPS was prepared by reacting powders of Li_2S and P_2S_5 in THF (99.9%, anhydrous, Sigma-Aldrich) under Ar, followed by treatment under vacuum at room temperature and subsequent heat treatment under vacuum at the designated temperature (80 °C or 140 °C). THF was dried using molecular sieves before use.[32] LPS-polymeric binder composites were prepared using the same wet-chemical method as for LPS, except that the polymers (5.5 wt%) were dissolved in THF solutions containing Li_2S and P_2S_5. A 5 g stoichiometric mixture of Li_2S, P_2S_5, and LiCl (99.99%, Sigma-Aldrich) in dibutyl ether (2 mL, 99.3%, Sigma-Aldrich) was mechanically milled at 600 rpm for 10 h in a zirconia vial (80 mL) with 15 zirconia balls (10 mm in diameter) to prepare the Li_6PS_5Cl (LPSCl) used as a separating SE layer in all-solid-state cells. After removing the solvent (dibutyl ether) under vacuum at 120 °C for 2 h, the dried powders were heat-treated at 550 °C for 5 h under Ar, resulting in a conductivity of 1.1×10^{-3} S cm^{-1} at 30 °C. The NCM622 powders were coated with $LiNbO_3$ (0.3 wt%) before use.[10]

Material characterization

XRD cells containing hermetically sealed samples with a beryllium window were mounted on a D8-Bruker Advance diffractometer equipped with Cu K_α radiation (0.154056 nm). FESEM images were obtained using S-4800 (Hitachi) or JSM-7000F (JEOL). Raman spectra were acquired with an Alpha300S (Witec Instrument) using a 532 nm Nd-YAG laser. Thermogravimetric analysis (TGA) experiments were carried out from 25 to 400 °C at 5 °C min^{-1} under Ar using a Q50 (TA Instrument Corp.).

Electrochemical characterization

Li-ion-blocking Ti/SE/Ti symmetric cells were assembled to measure the Li-ion conductivity of SE and SE-polymeric binder

This journal is © The Royal Society of Chemistry 2017

J. Mater. Chem. A, 2017, **5**, 20771–20779 | **20777**

pellets prepared by pressing at 370 MPa. AC impedance data were collected using an Iviumstat (IVIUM Technologies Crop.) in the range of 10 Hz and 1.5 MHz with an amplitude of 100 mV. The one-pot slurry for producing composite electrodes was prepared by stirring a mixture of the active material (NCM622 or graphite), Li_2S, P_2S_5, conducting agent (Super C65), and polymeric binder in THF under an Ar atmosphere overnight at room temperature. The weight ratios of active material : SE (LPS) : super C65 : binder were 70.0 : 27.5 : 1.0 : 1.5 for NCM622 electrode and 50.0 : 47.5 : 0.0 : 2.5 for graphite electrode, which corresponds with 47 vol% and 48 vol% of NCM622 and graphite electrodes, respectively. After the prepared slurry mixtures were spread on a piece of current collector foil (Al and Ni foils for the NCM622 and graphite electrodes, respectively) via a conventional doctor blade method, they were subjected to heat treatment at 140 °C under vacuum to remove the THF and promote crystallization of Li_3PS_4. $Li_{0.5}In$ (nominal composition) powders were prepared by mixing In (Aldrich, 99%) and Li (FMC Lithium Corp.) powders, and were used as the counter and reference electrodes.[29] All-solid-state half-cells (represented as electrode/SE/$Li_{0.5}In$) were assembled as follows. After forming a pellet of LPSCl (150 mg) by cold-pressing for use as a separating SE layer, the as-prepared electrodes, and $Li_{0.5}In$ powders were attached to opposite sides of the separating SE layer. Then, the assembled cells were pressed at 370 MPa at room temperature. The cathode (5.0 mg) and anode (4.7 mg) materials were each loaded in all-solid-state half-cells. The ~70 μm-thick SE-NW films were fabricated by embedding LPS powders (1.0 × 10^{-3} S cm^{-1}) into the porous structures of poly(paraphenylene terephthalamide) (PPTA) NW and densifying subsequently, as described in our previous report.[31] The NCM622/graphite ASLB was assembled by attaching the as-prepared NCM622 and graphite electrodes to the LPSCl separating SE layer (or the SE-NW film) and pressing at 370 MPa. A np ratio was ~2.4. The NCM622/graphite ASLBs at 30 °C were first cycled at 0.1C (17 mA g$_{NCM622}$$^{-1}$) for two cycles and then at 0.2C for a subsequent 13 cycles. The test temperature and C-rate were then raised to 100 °C and 15C, respectively. All assembly processes were performed in a polyaryletheretherketone (PEEK) mold (13 mm in diameter) and an Ar-filled glove box. Nyquist plots for the NCM622/Li–In cells were obtained after charging at 0.1C (40 μA cm^{-2}) to 4.3 V (vs. Li/Li$^+$) and resting for more than 3 h. The surface coverage of SEs onto NCM622 particles was obtained by dividing the apparent surface area of NCM622 particles (obtained by N_2 adsorption–desorption isotherm) by the contact area between NCM622 particles and SE (obtained by GITT analysis).[10] The GITT measurements were carried out with a pulse current of 0.1 mA cm^{-2} for 60 s and rest for 2 h.

Conflicts of interest

There are no conflicts to declare.

Acknowledgements

Notes and references

1 J. B. Goodenough and Y. Kim, *Chem. Mater.*, 2010, **22**, 587–603.

2 J.-M. Tarascon, *Philos. Trans. R. Soc., A*, 2010, **368**, 3227–3241.

3 N. Kamaya, K. Homma, Y. Yamakawa, M. Hirayama, R. Kanno, M. Yonemura, T. Kamiyama, Y. Kato, S. Hama, K. Kawamoto and A. Mitsui, *Nat. Mater.*, 2011, **10**, 682–686.

4 Y. Kato, S. Hori, T. Saito, K. Suzuki, M. Hirayama, A. Mitsui, M. Yonemura, H. Iba and R. Kanno, *Nat. Energy*, 2016, **1**, 16030.

5 Y. S. Jung, D. Y. Oh, Y. J. Nam and K. H. Park, *Isr. J. Chem.*, 2015, **55**, 472–485.

6 J. Janek and W. G. Zeier, *Nat. Energy*, 2016, **1**, 16141.

7 Y. Wang, W. D. Richards, S. P. Ong, L. J. Miara, J. C. Kim, Y. Mo and G. Ceder, *Nat. Mater.*, 2015, **14**, 1026–1032.

8 J. C. Bachman, S. Muy, A. Grimaud, H.-H. Chang, N. Pour, S. F. Lux, O. Paschos, F. Maglia, S. Lupart, P. Lamp, L. Giordano and Y. Shao-Horn, *Chem. Rev.*, 2016, **116**, 140–162.

9 Z. Yu, S.-L. Shang, J.-H. Seo, D. Wang, X. Luo, Q. Huang, S. Chen, J. Lu, X. Li, Z.-K. Liu and D. Wang, *Adv. Mater.*, 2017, **29**, 1605561.

10 K. H. Park, D. Y. Oh, Y. E. Choi, Y. J. Nam, L. Han, J.-Y. Kim, H. Xin, F. Lin, S. M. Oh and Y. S. Jung, *Adv. Mater.*, 2016, **28**, 1874–1883.

11 A. Banerjee, K. H. Park, J. W. Heo, Y. J. Nam, C. K. Moon, S. M. Oh, S.-T. Hong and Y. S. Jung, *Angew. Chem., Int. Ed.*, 2016, **55**, 9634–9638.

12 A. Sakuda, A. Hayashi and M. Tatsumisago, *Sci. Rep.*, 2013, **3**, 2261.

13 F. Mizuno, A. Hayashi, K. Tadanaga and M. Tatsumisago, *Adv. Mater.*, 2005, **17**, 918–921.

14 Y. Seino, T. Ota, K. Takada, A. Hayashi and M. Tatsumisago, *Energy Environ. Sci.*, 2014, **7**, 627–631.

15 H.-J. Deiseroth, S.-T. Kong, H. Eckert, J. Vannahme, C. Reiner, T. Zaiss and M. Schlosser, *Angew. Chem., Int. Ed.*, 2008, **47**, 755–758.

16 R. Murugan, V. Thangadurai and W. Weppner, *Angew. Chem., Int. Ed.*, 2007, **46**, 7778–7781.

17 R. Kanno and M. Murayama, *J. Electrochem. Soc.*, 2001, **148**, A742–A746.

18 B. R. Shin, Y. J. Nam, D. Y. Oh, D. H. Kim, J. W. Kim and Y. S. Jung, *Electrochim. Acta*, 2014, **146**, 395–402.

19 Y. Zhu, X. He and Y. Mo, *J. Mater. Chem. A*, 2016, **4**, 3253–3266.

20 A. Sakuda, A. Hayashi and M. Tatsumisago, *Chem. Mater.*, 2010, **22**, 949–956.

21 N. Ohta, K. Takada, L. Zhang, R. Ma, M. Osada and T. Sasaki, *Adv. Mater.*, 2006, **18**, 2226–2229.

22 Z. Liu, W. Fu, E. A. Payzant, X. Yu, Z. Wu, N. J. Dudney, J. Kiggans, K. Hong, A. J. Rondinone and C. Liang, *J. Am. Chem. Soc.*, 2013, **135**, 975–978.

20778 | *J. Mater. Chem. A*, 2017, **5**, 20771–20779

This journal is © The Royal Society of Chemistry 2017

23 E. Rangasamy, Z. Liu, M. Gobet, K. Pilar, G. Sahu, W. Zhou, H. Wu, S. Greenbaum and C. Liang, *J. Am. Chem. Soc.*, 2015, **137**, 1384–1387.

24 R. C. Xu, X. H. Xia, Z. J. Yao, X. L. Wang, C. D. Gu and J. P. Tu, *Electrochim. Acta*, 2016, **219**, 235–240.

25 F.-D. Han, J. Yue, X. Fan, T. Gao, C. Luo, Z. Ma, L. Suo and C. Wang, *Nano Lett.*, 2016, **16**, 4521–5427.

26 Y. E. Choi, K. H. Park, D. H. Kim, D. Y. Oh, H. R. Kwak, Y.-G. Lee and Y. S. Jung, *ChemSusChem*, 2017, **10**, 2605–2611.

27 D. He and N. N. Ekere, *J. Phys. D: Appl. Phys.*, 2004, **37**, 1848–1852.

28 B. R. Shin, Y. J. Nam, J. W. Kim, Y. G. Lee and Y. S. Jung, *Sci. Rep.*, 2014, **4**, 5572.

29 D. Y. Oh, Y. E. Choi, D. H. Kim, Y.-G. Lee, B.-S. Kim, J. Park, H. Sohn and Y. S. Jung, *J. Mater. Chem. A*, 2016, **4**, 10329.

30 J. E. Trevey, C. R. Stoldt and S. H. Lee, *J. Electrochem. Soc.*, 2011, **158**, A1282–A1289.

31 Y. J. Nam, S. J. Jo, D. Y. Oh, J. M. Im, S. Y. Kim, J. H. Song, Y. G. Lee, S. Y. Lee and Y. S. Jung, *Nano Lett.*, 2015, **15**, 3317–3323.

32 T. Inada, K. Takada, A. Kajiyama, M. Kouguchi, H. Sasaki, S. Kondo, M. Watanabe, M. Murayama and R. Kanno, *Solid State Ionics*, 2003, **158**, 275–280.

33 S. Ito, S. Fujiki, T. Yamada, Y. Aihara, Y. Park, T. Y. Kim, S.-W. Baek, J.-M. Lee, S. Doo and N. Machida, *J. Power Sources*, 2014, **248**, 943–950.

34 D. H. Kim, D. Y. Oh, K. H. Park, Y. E. Choi, Y. J. Nam, H. A. Lee, S.-M. Lee and Y. S. Jung, *Nano Lett.*, 2017, **17**, 3013–3020.

35 D. Y. Oh, Y. J. Nam, K. H. Park, S. H. Jung, S.-J. Cho, Y. K. Kim, Y.-G. Lee, S.-Y. Lee and Y. S. Jung, *Adv. Energy Mater.*, 2015, **5**, 1500865.

36 J. F. Rabek, Y. J. Shur and B. Ranby, *J. Polym. Sci., Polym. Chem.*, 1975, **13**, 1285–1295.

37 K. Homma, M. Yonemura, T. Kobayashi, M. Nagao, M. Hirayama and R. Kanno, *Solid State Ionics*, 2011, **182**, 53–58.

38 Y. Furukawa, H. Ohta, A. Sakamoto and M. Tasumi, *Spectrochim. Acta, Part A*, 1991, **47**, 1367–1373.

39 H. Visbal, Y. Aihara, S. Ito, T. Watanabe, Y. Park and S. Doo, *J. Power Sources*, 2016, **314**, 85–92.

40 H. Kim, M. G. Kim, H. Y. Jeong, H. Nam and J. Cho, *Nano Lett.*, 2015, **15**, 2111–2119.

41 Y. S. Jung, A. S. Cavanagh, L. A. Riley, S. H. Kang, A. C. Dillon, M. D. Groner, S. M. George and S. H. Lee, *Adv. Mater.*, 2010, **22**, 2172–2176.

42 Y. S. Jung, P. Lu, A. S. Cavanagh, C. Ban, G. H. Kim, S. H. Lee, S. M. George, S. J. Harris and A. C. Dillon, *Adv. Energy Mater.*, 2013, **3**, 213–219.

43 J. W. Kim, D. H. Kim, D. Y. Oh, H. Lee, J. H. Kim, J. H. Lee and Y. S. Jung, *J. Power Sources*, 2015, **274**, 1254–1262.

44 J. Billaud, F. Bouville, T. Magrini, C. Villevieille and A. R. Studart, *Nat. Energy*, 2016, **1**, 16097.

45 J. Landesfeind, J. Hattendorff, A. Ehrl, W. A. Wall and H. A. Gasteiger, *J. Electrochem. Soc.*, 2016, **163**, A1373–A1387.

46 Y. Yamada, K. Furukawa, K. Sodeyama, K. Kikuchi, M. Yaegashi, Y. Tateyama and A. Yamada, *J. Am. Chem. Soc.*, 2014, **136**, 5039–5046.

47 K. Xu, *Chem. Rev.*, 2004, **104**, 4303–4417.

This journal is © The Royal Society of Chemistry 2017

J. Mater. Chem. A, 2017, **5**, 20771–20779 | **20779**